AN ARX MODEL APPROACH TO fNIRS DATA ACQUIRED FROM MIGRAINE AND HEALTHY SUBJECTS

by

Esin Karahan

B.S., in Electrical & Electronics Engineering, Boğaziçi University, 2005

Submitted to the Institute of Biomedical Engineering
in partial fulfillment of the requirements
for the degree of
Master of Science
in
Biomedical Engineering

Boğaziçi University
August 2007

AN ARX MODEL APPROACH TO fNIRS DATA ACQUIRED FROM MIGRAINE AND HEALTHY SUBJECTS

APPROVED BY:

Asst.Prof. Ata Akın .....
(Thesis Advisor)

Prof. Dr. Ahmet Ademoğlu .....

Prof. Dr. Hayrünnisa Bolay .....

DATE OF APPROVAL: 08.08.2007

ACKNOWLEDGMENTS

I would like to thank my supervisor Dr. Ata Akın, for his generous guidance and support in all the time of research for and writing of this thesis. He was always helpful in my problems relating thesis.

I am grateful to Prof. Dr. Ahmet Ademoğlu for his valuable contributions at various occasions. I am thankful to Prof. Dr. Hayrünnisa Bolay for her help in providing data from migraine subjects.

I would like to express my gratitude to Nermin Topaloğlu, Sinem Burcu Erdoğan and Sinem Serap for their help and encouragement to go ahead with my thesis. I extend my thanks to Onur Güngör and Abuzer Yakaryılmaz for their help.

I am deeply indebted to Özer, İrem and Azime whose moral support encouraged me through this period. Their continued friendship motivated me all the time.

I would like to give my special thanks to my family for their endless altruism, patience and support throughout my whole life.

ABSTRACT

AN ARX MODEL APPROACH TO fNIRS DATA ACQUIRED FROM MIGRAINE AND HEALTHY SUBJECTS

This study is focused on investigating the cerebrovascular dynamics of migraine by analyzing data acquired from healthy and migraine subjects with a non-invasive measuring technique, fNIRS during a breath holding task. Brain hemodynamic responses of subjects are modeled via a parametric identification technique, Auto-regressive with Exogenous input (ARX) model. Analysis of modeled signals for healthy and migraine subjects is performed both in frequency and time domains. In frequency domain analysis, frequency intervals in which power spectrum estimates of migraineurs significantly differ from healthy ones, are obtained as 0.01-0.03Hz, around 0.13 Hz and higher than 0.2 Hz ($p<0.05$). The energy of the estimated signals of migraineurs in 0.01-0.03 Hz is approximately five folds smaller than the healthy ones, whereas in 0.13 Hz and 0.25 Hz this difference is approximately 1.5 folds. Time domain analysis has shown that the amplitude of peak response of migraineurs is five folds smaller than the healthy ones during all breath holding procedure ($p<0.05$). Required model orders to fulfill the dynamics of response are found higher in migraine case. Results obtained show that response of cerebrovascular system of migraine subjects to breath holding task is considerably different with respect to normal subjects.

Keywords: Migraine, Cerebrovascular Dynamics, Functional Near Infrared Spectroscopy (fNIRS), Linear Parametric Identification, Autoregressive Exogenous Input (ARX) Model.

ÖZET

NORMAL VE MİGRENLİ DENEKLERDEN İŞLEVSEL YAKIN KIZIL ÖTESİ SPEKTROSKOPİ İLE ALINAN ÖLÇÜMLERİN ARX MODELLEME YAKLAŞIMI İLE İNCELENMESİ

Bu çalışma, migrenli ve sağlıklı deneklerden invazif olmayan bir ölçme yöntemi olan İYKÖS ile alınan bilgiyi analiz ederek migren hastalığının cerebrovasküler dinamiklerini incelemeyi amaçlamaktadır. Deneklerin beyin hemodinamik cevapları parametrik bir tanılama yöntemi olan özbağlanımlı dışyapılı modelle modellenmiştir. Sağlıklı ve migrenli deneklerin modellenmiş sinyallerinin analizi frekans ve zaman bölgelerinde yapılmıştır. Frekans bölgesi analizinde, migrenli deneklerin modellenmiş güç spektrumunun 0.01-0.03 Hz, 0.13 Hz civarında ve 0.2 Hz'den büyük frekanslarda sağlıklı deneklerin modellenmiş güç spektrumuna göre farklılık gösterdiği bulunmuştur ($p<0.05$). Migrenlilere ait tahmini sinyallerin enerjileri 0.01-0.03 Hz frekans aralığında sağlıklı olanlarinkine göre 5 kat, 0.13 Hz ve 0.2 Hz frekanslarında ise 1.5 kat daha küçüktür. Zaman bölgesi analizi, migrenlilerin cevaplarının tepe noktası değerinin sağlıklı deneklerin cevaplarına göre beş kat daha küçük olduğunu göstermiştir ($p<0.05$). Ayrıca, hemodinamik cevabı modellemek için gereken model dereceleri migrenli deneklerde daha yüksek bulunmuştur. Bu çalışma sonunda elde edilen sonuçlar migrenli deneklerin nefes tutma prokolüne verdikleri serebrovasküler cevapların normal deneklere göre farklı olduğunu göstermiştir.

Anahtar Sözcükler: Migren, Serebrovasküler Dinamikler, İşlevsel Yakın Kızılötesi Spektroskopi (iYKÖS), Doğrusal Parametrik Tanılama, Özbağlanımlı Dışyapılı Model.

TABLE OF CONTENTS

ACKNOWLEDGMENTS iii
ABSTRACT iv
ÖZET v
LIST OF FIGURES viii
LIST OF TABLES x
LIST OF SYMBOLS xi
LIST OF ABBREVIATIONS 1
1. INTRODUCTION 2
1.1 Motivation and Objectives 2
1.2 Outline of the Thesis 3
2. MIGRAINE 4
2.1 Definition 4
2.2 Diagnosis of Migraine 5
2.3 Pathophysiology of Migraine 6
2.3.1 Vascular Theory 7
2.3.2 Neurogenic Theory 7
2.3.2.1 The Meninges 7
2.3.2.2 The Trigeminovascular System 8
2.4 Functional Neuroimaging In Migraine 11
3. FUNCTIONAL NEAR INFRARED SPECTROSCOPY 12
3.1 fNIRS in Migraine Imaging 14
4. METHOD 15
4.1 Experimental Procedure 15
4.2 fNIRS Data Collection 15
4.3 Data Preprocessing 16
4.4 System Identification and Modeling 16
4.5 ARX Model 18
4.5.1 Determining Input and Output Signals of the ARX Model . . . 22
4.5.2 ARX Modeling Scheme-1 24

4.5.3 ARX Modeling Scheme-2 24
4.5.4 ARX Modeling Scheme-3 26
5. RESULTS AND DISCUSSION 29
5.1 Results from ARX Modeling Scheme-1 29
5.2 Results from ARX Modeling Scheme-2 36
5.3 Results from ARX Modeling Scheme-3 37
6. CONCLUSIONS 44
6.1 Recommendations for future work 44
REFERENCES 45

LIST OF FIGURES

Figure 2.1	The meninges [1]	8
Figure 2.2	The trigeminovascular system	10
Figure 3.1	The absorption spectrum of chromophores	13
Figure 4.1	Niroxcope 201 probe: Source-detector locations	16
Figure 4.2	Algorithm for the system identification	18
Figure 4.3	Block diagram of ARX model	19
Figure 4.4	Input and output signals of the ARX models. (a) Hb signal taken from fourth detector of fNIRS from a normal subject and corresponding hypothetical input signal and (b) Hb signal taken from third detector of fNIRS from a migraine subject and corresponding hypothetical input signal	23
Figure 4.5	Block diagram of the ARX modeling scheme 1	25
Figure 4.6	Block diagram of the ARX modeling scheme 3: $s(k)$ is the filtered version of average reference signal, $n(k)$ denotes modeled background activity	27
Figure 4.7	Measured [Hb] data from 12. detector during normal breathing	27
Figure 5.1	Model fit plots of [Hb] data taken from 14. detector during first (a,c) and second (b,d) breathholds for healthy (a,b) and migraine (c,d) subjects	30
Figure 5.2	Demonstration of statistically significant frequencies based on 16 detector recordings for each breath hold	32
Figure 5.3	Average power spectrum from healthy and migraine Patients	35
Figure 5.4	Overlapping frequencies in four breath holds. Pink colored cells are the mutual frequencies where at least three breath holds show significant differences. The energy of the each overlapping interval is denoted on the left for normals and migraneurs	36
Figure 5.5	Residual check performed on (a) estimation data and (b) validation data	37

Figure 5.6 Measured and filtered responses. (a) Hb signal taken from 12. detector of fNIRS from a normal subject and corresponding filtered signal and (b) Hb signal taken from 4. detector of fNIRS from a migraine subject and corresponding filtered signal 40

Figure 5.7 Modeled background activity for 13. detectors of normal and migraine subjects 40

Figure 5.8 Power spectrum of modeled background activity for migraine and healthy subjects 41

LIST OF TABLES

Table 5.1	Significant frequency intervals and corresponding sum of estimated power spectrums	33
Table 5.2	Orders of selected models for healthy and migraine subjects for each breath hold episodes	38
Table 5.3	Averaged orders of models for healthy and migraine subjects	39
Table 5.4	Amplitude values of averaged [Hb] data obtained from parametric identification for four breath holds (mean(std))	42
Table 5.5	Time to peak values of averaged [Hb] data obtained from parametric identification for four breath holds (mean(std))	43

LIST OF SYMBOLS

$ATPase$	Adenosine Tri-Phosphatease
B	Differential Pathlength Factor
c	Concentration
d	Path Length
Fs	Sampling Frequency
G	Signal Loss
Hb	Deoxy-hemoglobin
HbO_2	Oxy-hemoglobin
I_0	Incident Light Intensity
I	Transmitted Light Intensity
K	Potassium Ion
Na	Sodium Ion
$G(q)$	Transfer Function from Input to Output
$H(q)$	Transfer Function from White Noise to Output
n_a	Number of a Parameters
n_b	Number of b Parameters
q	Shift Operator
n_k	Delay
n	Model Order for Exogenous Part
m	Model Order for Autoregressive Part
$e(t)$	White Noise
$n(k)$	Modeled Background Activity
$s(k)$	Filtered Version of Reference Signal
$u(t)$	Output Variable at time t
$y(t)$	Output Variable at time t
$\hat{y}(t)$	Predicted Output at time t
$\overline{y}(t)$	Mean of Output Over Time Interval
V_N	Criterion Function

$Z_{est}^{N_1}$	Estimation Data Set
$Z_{val}^{N_2}$	Validation Data Set
ε	Exctinction Coefficient
$\varepsilon(t)$	Prediction Error
ϕ	Regression Vector
θ	Parameter Vector

LIST OF ABBREVIATIONS

ANOVA	Analysis of Variance
AR	Autoregressive
ARX	Autoregressive Exogenous Input Model
BHR	Brain Hemodynamic Response
CGRP	Calcitonin Gene Related Peptide
CSD	Cortical Spreading Depression
EEG	Electroencephalography
FHM	Familial Hemiplegic Migraine
fMRI	Functional Magnetic Resonance Imaging
fNIRS	Functional Near Infrared Spectroscopy
LF	Low Frequency
IHS	International Headache Society
HF	High Frequency
MRI	Magnetic Resonance Imaging
NIR	Near Infrared
PET	Positron Emission Tomography
std	Standard Deviation
V1	Opthalmic Branch of Trigeminal Nerve
V2	Maxillary Branch of Trigeminal Nerve
V3	Mandibular Branch of Trigeminal Nerve
VLF	Very Low Frequency

1. INTRODUCTION

1.1 Motivation and Objectives

Migraine is a complex neurovascular disorder characterized by recurrent and disabling headaches manifesting in attacks lasting 4-72 hours. A migraine attack has a moderate or severe intensity, aggravated by physical activity and associated with nausea, photophobia and phonophobia. Stress, emotional changes, altered sleep pattern, some foods and drugs trigger migraine. Nearly 12% of world's population suffers from migraine which restrains patients from daily activity and upset during attacks. Beside economic burden of medical costs for treatment, migraine disables patients from work and decreases the life quality of sufferers. Since the underlying mechanisms of migraine have not been fully understood, diagnosis of migraine is still a challenging subject.

This study is focused on investigating the cerebrovascular dynamics of migraine by using a measurement technique which quantifies the tissue oygenation. Data taken from migraine and healthy subjects during a breath hold task, are analyzed with single input single output parametric model (Autoregressive with Exeganous Input (ARX)). ARX models have been applied on biomedical signals specifically on EEG and fMRI signals because of the low signal to noise ratio of these signals. In this study, ARX model parameters and the frequency response of the estimated models are compared for two experiment groups. Different ARX modeling schemes are applied to be capable of model the whole process. It is intended to find significant differences in the result of modeling between two groups which will be useful in the analysis of cerebrovascular dynamics.

1.2 Outline of the Thesis

In this study, it is attempted to give a general information about migraine and measurement system used. I tried to apply a mathematical parametric identification technique for the analysis of cerebrovascular dynamics of migraineurs.

In Chapter 2, physiology and medical background of migraine is explained briefly by summarizing different approaches to elucidate the underlying mechanisms of migraine. Neuroimaging tools used for research and diagnosis of migraine are mentioned in the end of the second chapter.

Chapter 3 gives an introduction for the physical and mathematical basis of functional near infrared spectroscopy (fNIRS). Recent studies on migraine imaging with fNIRS are reviewed.

Chapter 4 begins with the experimental procedure and data collection. A brief explanation of system identification and Auto Regressive Exogenous model is followed with introduction of modeling schemes applied on the measured data.

The results of modeling procedures are presented in Chapter 5. Results are discussed in the frame of differences in cerebrovascular responses of migraine and normal subjects.

Chapter 6, gives a general discussion of the study and ends with the recommendations to validate and improve the results obtained.

2. MIGRAINE

Headaches are classified in two broad categories: primary headaches and secondary headaches. Primary headaches which are not caused by organic or structural diseases include migraine, cluster headaches, tension-type headaches and the other types. Secondary headaches are the result of underlying structural or organic diseases ranging from brain tumours to head or neck injuries, sinus infections, abnormalities of the spinal fluid. More than 90 % of headaches are primary headaches. Migraine is the second common primary headache type after cluster headaches [2].

2.1 Definition

Migraine is a complex neurobiological disorder characterized by throbbing head pain usually sensed greater on one side of the brain. Migraine affects 2-15% of the world's population leading periodic or unpredictable disability. A migraine attack is described by four main phases to classify signs and symptomps: prodrome, aura, pain and postdrome phases. The phases are not experienced by all migraineurs and also vary from one migraine attack to another in the same patient. The *prodrome* phase experienced by 60 % of migraineurs, begins hours or up to 2 days before the headache, exhibiting typical symptoms such as depression, fatigue, yawning, food craving, hypersensitivity to light, sound or smell. Prodrome phase is preceded with the *aura* phase indicating focal cerebral, cortical and/or brainstem dsyfunction. Typical aura symptoms are grouped in two: visual and neurological. Visual symptoms include flashing lights, shimmering zigzag lines and blind spots whereas neurological ones include paresthesia, numbness, unilateral weakness and speech disturbance (aphasia). The aura experienced by 20% of migraneurs, gradually develops over 5-20 minutes and usually lasts less than 60 minutes. In the *pain* phase, migraineurs suffer severe headache lasting from four hours to two or three days. Headache is typically unilateral, pulsating and accompanied with nausea, photophobia and phonophobia, sometimes vomiting, and worsened by physical activity. The *postdrome* phase is a time for recovery and is

characterized by impaired concentration, scalp tenderness, tiredness, exhaustion and mild headache [2].

2.2 Diagnosis of Migraine

Diagnosis of migraine has been improved with the publishment of consensus set of diagnostic criteria for two main subtypes of migraine; migraine with aura and migraine without aura by the International Headache Society (IHS). Although the criteria are not perfect, they are accepted as more informative and reliable than prior techniques. The criteria helps to distinguish migraine from other two common headaches disorders, tension- and cluster-type. Migraine without aura termed as common migraine is seen in 80% of migraine sufferers and typified by at least 5 attacks lasting 4-72 hours. According to IHS criteria, attacks are unilateral, pulsating quality, qualified as moderate to severe intensity and aggravated by routine physical activity. During headache, at least one of three symptoms as nausea and/or vomiting, photophobia and phonophobia and no evidence of related organic disease is required. Migraine with aura termed as classic migraine is a recurring headache associated with reversible focal neorological symptoms. Migraine with aura is subdivided in six categories for diagnosis: migraine with typical aura, migraine with prolonged aura, familial hemiplegic migraine, basilar migraine, migraine aura without headache and migraine with acute onset aura. For the diagnosis of migraine without aura, there must have been at least 2 attacks not attributable to another organic disease. At least 3 of 4 symptoms specified by IHS should be fulfilled: one or more completely reversible aura symptoms that indicate focal cerebral cortical or brain-stem dysfunction (or both) , at least one aura symptom develops gradually over more than 4 minutes or two or more symptoms occur in succession, no aura symptom lasts longer than 60 minutes and headache follows aura in one hour. Furthermore at least one of aura features should be experienced: homonymous visual disturbance, unilateral paresthesis and/or numbness, unilateral weakness and aphasia or unclassifiable speech difficulty [2, 3].

For an accurate method that satisfies the IHS criteria in diagnosis of migraine

clinical history, physical and neurological features should be investigated. Age of onset, family history, duration, character and intensity of pain, mode of onset, time between onset to peak pain, temporal profile, aggravating or precipitaining factors should be elicited [4]. The general physical examination evaluates at least the following: vital signs such as blood pressure and heart rate; cardiac status; extracranial structures; range of motion and the presence of pain in the cervical spine [5]. Neurological examinations are performed for detecting headaches due to intracranial or systemic diseases. Neuroimaging techniques provide a better understanding of the neuroanatomical and physiological basis of the conditions [6].

2.3 Pathophysiology of Migraine

Researches on migraine have been augmented over the past few decades. Nevertheless pathophysiological mechanism underlying a migraine attack is not fully understood. General opinion in migraine is the neuronal hyperexcitability to both genetic and environmental factors which determine the threshold for triggering attacks [7]. It is hypothesized that anyone can have a migraine attack initiated by migraine specific triggers. However recurrement of attacks is related to the lowered threshold and the frequency or intensity of the triggers. Genetic factors leading abnormality in ion-channel function lower the threshold and internal and environmental factors including allergic reactions, sensitivity to light, sound and certain foods, stress, changes in sleep pattern and hormonal fluctuations affect the occurence of migraine [8].

Several theories have been proposed to elucidate the physiological events occurring onset and during a migraine attack. Migraine has been long regarded as a vascular disorder caused by vasodilation of blood vessels. However recent researches show evidences interrogating this theory by making a connection between central nervous system and blood vessels. The two main hypotheses explaining the pathophysiology of migraine are vascular theory and neurogenic theory.

2.3.1 Vascular Theory

In the 1940s and 1950s, Wolff et al. proposed that intracranial vasoconstriction is responsible for the aura of migraine and that the subsequent rebound vasodilatation and activation of perivascular nociceptive nerves resulted in headache. This theory was based on the observations that extracranial vessels become distended and pulsatile during a migraine attack; stimulation of intracranial vessels in an awake person induces headache; and vasoconstrictors such as ergots improve the headache, whereas vasodilators such as nitroglycerin provoke an attack [9]. However, some studies have shown that headache phase of migraine with aura starts while blood flow is reduced [10]. Furthermore, vasodilation alone cannot explain the local swelling and tenderness of the headache that generally accompany migraine [11].

2.3.2 Neurogenic Theory

The neurogenic theory of migraine states that a complex series of neural and vascular events initiate migraine challenging the early claims linking headache pain with simply vasodilation. Migraneurs have a central neuronal hyperexcitability as a physiological disturbance predisposing migraine [12]. Before proceeding in neurogenic theory, two important physiological units; meninges and trigeminal nerve will be mentioned which are important in pathophysiology of the migraine linking the trigeminal innervation of cranial vessels.

2.3.2.1 The Meninges. The meninges are a series of three membranes covering the brain and spinal cord that act to protect and partition the central nervous system. The membranes comprising the meninges are the dura mater, arachnoid layer, and the pia mater. The outer layer, the *dura mater*, is composed of dense fibrous tissue which supports and surrounds large venous channels (dural sinuses). The more superficial layer of dura mater is called periosteal layer which attaches to the periosteum of the cranial bones. The meningeal layer of the dura mater lies deep to the periosteal

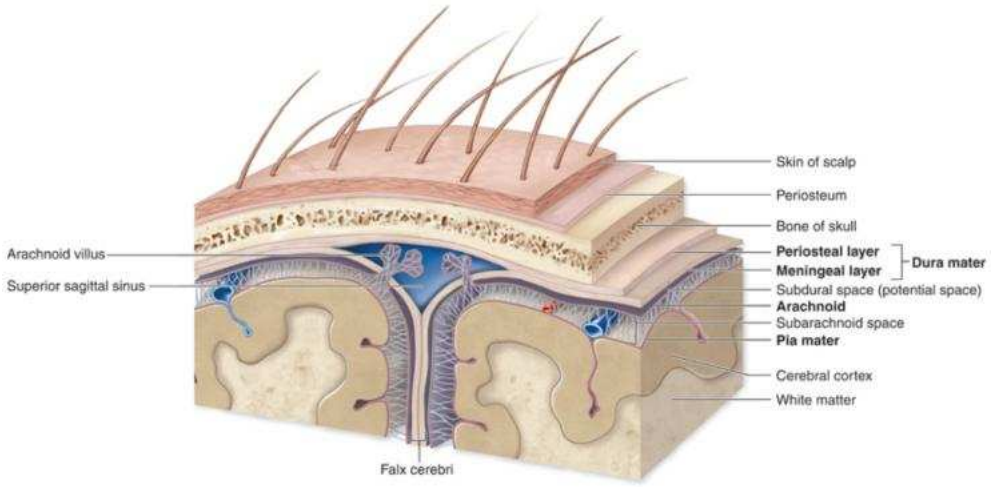

Figure 2.1 The meninges [1]

layer. Two layers separate in dural venous sinuses to form large, blood filled spaces. *Arachnoid matter* lying underneath of the dura matter is composed of delicate web of collagen and elastic fibers. The space between the arachnoid and the overlying dura mater is the subdural space which is absent in the walls of large venous channels of the dura matter. Penetration of arachnoid in the dura matter and projection into veins is referred as arachnoid villi or arachnoid granulations. From arachnoid villi, cerebrospinal fluid passes from the subarachnoid space to the venous blood. The *pia matter* is the innermost layer of the meninges. It is a thin layer of delicate connective fibrous tissue and tightly adheres to brain following all contours of brain. Blood vessels piercing the pia matter nourishes the brain. The pia and arachnoid are not separate layers and sometimes together they are called the leptomeninges [1].

2.3.2.2 The Trigeminovascular System. The trigeminal nerve is the fifth of twelve cranial nerves and is composed of three large nerve branches: ophthalmic (V1, sensory), maxillary (V2, sensory) and mandibular (V3, motor and sensory) branches. All sensations from the face and mouth namely discriminative touch, proprioception, pain and temperature are covered by the mixed trigeminal nerve. The three branches of the trigeminal nerve converge on the trigeminal ganglion from where the trigeminal nerve courses backward to enter the mid-lateral aspect of the pons part of brain stem. Immediately adjacent to the sensory root, a smaller motor root emerges from the pons

at the same level. Branchial motor nerves exit the mid-lateral aspect of the pons, course within the trigeminal nerve, pass through the trigeminal ganglion, and exit the middle cranial fossa within the mandibular nerve through foramen ovale. All sensory fibers from the face terminate in the trigeminal nucleus and send projections via the thalamus to primary sensory cortices in cerebral cortex for higher order processing.

Branches of the ophthalmic nerve (V1) convey sensory information from the skin of the forehead, upper eyelids, and lateral aspects of the nose and provides sensory innervation to the eyeball structures, nasal mucosa, and cutaneous areas around the eye, the dorsum of the nose and the frontal area. Branches of the maxillary nerve (V2) convey sensory information from the lower eyelids, zygomae, and upper lip. Branches of the mandibular nerve (V3) convey sensory information from the lateral scalp, skin anterior to the ears, lower cheeks, lower lips, and anterior aspect of the mandible. Its function is to provide sensory innervation to the rostral 2/3 of the tongue, skin of the intermandibular area, skin on the concave surface of the ear, and skin on the cheek. Also maxillary nerve provides motor innervation to the muscles of mastication [13, 14, 15].

Beside conveying sensory information from face and mouth, small calibre trigeminal axons innervates the meninges and bifurcate near small blood vessels branching from the pial and dural arteries. Innervation of meninges and the cerebral and intracranial vessels by the trigeminal nerve forms the trigeminovascular system (Fig. 2.2). Sensory information from the trigeminovascular system is carried through the ophthalmic branch of the trigeminal nerve. Trigeminal nerve fibers are situated at the interface between blood and cerebrospinal fluid or brain parenchyma, possibly to detect the presence of any noxious substances originating from these sources. Sensitization or activation of trigeminovascular afferents release vasoactive neuropeptides: calcitonin gene-related peptide (CGRP), substance P and neurokinin A that mediate vasodilation and edema [16]. Innervation of blood vessels in dura matter by peripheral afferent fibers of trigeminal system points out that this part is sensitive to pain and neurogenic inflammation within dura matter constitutes the grounds of the neurogenic hypothesis. Activation of trigeminovascular system leads to release of inflammatory and vasodila-

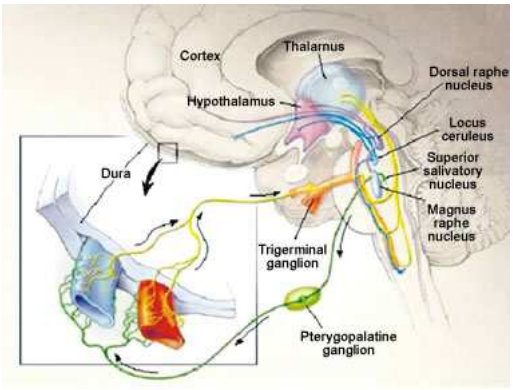

Figure 2.2 The trigeminovascular system

tory neuroactive susbtances. These substances cause vasodilation and extravasation of plasma proteins from peripheral meningeal vessels and induce nociceptors to facilitate headache [16]. Some researches have been supported that CGRP levels in jugular vein of patients increased during migraine attacks [17]. Furthermore, stimulation of meningeal primary afferent neurons in the trigeminal ganglion followed by stimulation of central trigeminocervical neurons causes the nociceptive fibers sensitive to arterial pulse and head movements. Hypersensitivity could mediate the throbbing pain of migraine and its worsening during coughing, bending over, or other physical activities that increase intracranial pressure [18].

It has been hypothesized that cortical spreading depression (CSD) which is characterized as a wave of depolarization that propagates slowly across the cortex, depressing neuronal activity for a few minutes and transiently increases cerebral blood flow followed by vasoconstriction, initiates migraine headache [19]. CSD is first described by Leao that a migraine aura is due to a wave of neuronal excitation in the cortical gray matter that spreads across cerebral cortex at the rate of 2-6 mm/min [20]. Recent studies with imaging techniques like MRI have been shown a link between CSD and migraine aura. Recordings within occipital cortex during visual aura have shown that aura is accompanied by a propagating event which is moving from central to peripheral visual fields [21].

Triggering mechanisms of CSD in human cortex during migraine have not been

fully understood. Cortical trauma, exposure to high excitatory amino acid and potassium ion, direct electrical stimulation, inhibition of Na+/K+-ATPase and energy failure may trigger CSD. Genetic and environmental factors may represent risk by lowering the CSD threshold and cortical excitation may cause sufficient elevation in extracellular K+ and glutamate to initiate CSD [22]. In the case of Familial Hemiplegic Migraine (FHM) type 1, a gene mutation is found in the P/Q type calcium channel which controls release of the excitatory amino acid, glutamate in the synaptic cleft. In the case of FHM type 2 gene mutation occurs in the Na/K ATPase enzyme. Accumulation of glutamate or potassium ions in the synaptic cleft initiates CSD [19].

2.4 Functional Neuroimaging In Migraine

Diagnosis of primary headaches including migraine is a clinical task. Although some researches propose that migraineurs are under increased risk for subclinical lesions in certain areas relative to non migraineurs, it is still a controversial issue [23]. However, recently functional neuroimaging techniques let a better understanding of pathophysiology of migraine. With the introduction of neurogenic theory, it has been proposed that migraine pain leads neural function in trigeminovascular system. The trigeminal ganglion, spinal trigeminal nucleus and the somatosensory cortex constituting the nociceptive pathway in humans, could be imaged via a non-invasive neuroimaging technique, functional magnetic resonance imaging (fMRI) [24]. fMRI measures changes in blood flow by using differences in paramagnetic properties of hemoglobin and deoxyhemoglobin. Change in blood flow is considered as the change in neural activity. Activation during a migraine attack are mapped on to anotomical brain images which provide assessment to active brain regions [24]. Another neuroimaging technique, positron emission tomography (PET) which requires injection of labeled radioactive isotopes to blood, provides the quantative measurement of regional cerebral blood flow and can elucidate imaging of active brain regions.

3. FUNCTIONAL NEAR INFRARED SPECTROSCOPY

Near infrared spectroscopy (NIRS) is a non-invasive method for determination of changes in regional cerebral oxygenation and hemodynamics within the brain. Recently, measuring the cerebral blood flow and cerebral blood volume is possible by using near infrared light [25, 26]. NIRS measurement is based on the absorption of near infrared lights proportional to concentrations of oxy-hemoglobin and deoxy-hemoglobin.

In 1977, Jobsis [27] first demonstrated that changes in oxygenation of brain could be monitored by near infrared radiation. NIR light when exposed on head can penetrate the scalp and skull and is attenuated within the tissue. Attenuation of the near infrared light in tissue is described with Beer-Lambert law:

$$\log(I_0/I) = \varepsilon \cdot c \cdot d \tag{3.1}$$

where I_0 is the incident light intensity, I is the transmitted light intensity, ε is the specific extinction coefficient of the compound, c is the concentration of the compound, and d is the length of the light path through tissue.

Attenuation of NIR light in tissue is due to light scattering of cellular and sub cellular compartments and absorption of certain compounds of tissue called chromopheres. Important tissue chromophores are melanin, myoglobin water, hemoglobin and cytochrome oxidase. Melanin is the pigment of epidermal layer of human skin which absorbs NIR light also. Since its concentration does not change during measurement, its effect can be compensated in difference computation of concentration. Myoglobin is the primary oxygen carrying pigment of muscle tissues. Unlike the hemoglobin, the binding of oxygen by myoglobin is unaffected by the oxygen pressure in the surrounding tissue. Absorption of light of hemoglobin varies with its oxygenation status. In the near infrared region between 650-1000nm, water has a lesser absorption level compared to hemoglobin. This transperancy window allows NIR light to penetrate tissue to illuminate deeper structures such as cerebral cortex (Fig. 3.1). From that

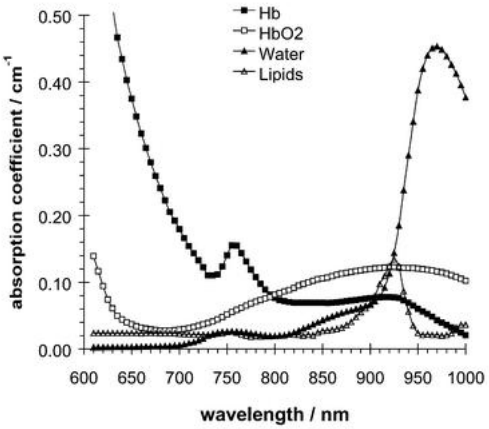

Figure 3.1 The absorption spectrum of chromophores

point, concentration changes of oxyhemoglobin and deoxyhemoglobin which together give the regional oxygenation information can be measured based on light absorption measurement.

Beer-Lambert law can be applied on stituations where attenuation of light is only due to absorption or direct transmission. Since absolute attenuation in tissue can not be determined due to scattering, calculation of absolute hemoglobin concentration can not be achieved. In order to overcome this difficulty, quantative measurements in near infrared spectroscopy is based on the modified Beer-Lambert's law [28]:

$$A = \varepsilon \cdot c \cdot d \cdot B + G \tag{3.2}$$

where B is the differential pathlength factor and G is the signal loss due to light scattering. By using Equation 3.2 scattering of light is embedded in pathlength of light through tissue. Differential pathlength factor represents the increase in distance traveled by light and can be calculated [29]. Because of unknown factor G, the solution of the Equation 3.2 cannot provide a measure of the total concentration of the chromophore in the medium. However, on the assumption that tissue geometry is unchanged during measurement, change in the chromophore concentration can be determined from the changes in light attenuation.

3.1 fNIRS in Migraine Imaging

In recent years, fNIRS studies have been become widespread in brain activity researches associated with cerebral hemodynamics changes. Since there has been general belief that migraine is a neurovascular disorder, investigating the cerebrovascular responses of migraineurs with neuroimaging tools has been an interesting topic. In this section only studies that used fNIRS in migraine imaging will be summarized.

A study performed by Akın *et al.* which inspired this work, has shown the cerebrovascular dynamics of migraine during breath holding task. Both deoxyhemoglobin and oxyhemoglobin signals are evaluated using a mathematical gaussian function [30]. In a similar study differences in the peak and latencies of the initial dip and recovery phases for deoxyhemoglobin and oxyhemoglobin signals during breath holding for migraine and healthy subjects have been demonstrated [31]. A recent study combining transcranial Doppler and NIRS, compares the cerebral blood flow velocity and concentrations of oxyhemoglobin and deoxyhemoglobin of migraine and healthy subjects where subjects are performing a breath holding task. It has been found that cerebral blood flow velocity of migraneurs does not show significant differences in baseline conditions whereas during the breath holding task there exists a dispersion between two groups [32]. Shinoura *et al.* conducted a head-down maneuver experiment on migraine and healthy subjects in order to compare the changes in total hemoglobin and regional oxygen saturation of the right and left frontal lobes. Results of the study show that increase in right-sided total hemoglobin concentration of migraneurs is smaller than healthy subjects whereas on the left side no difference is seen. The change in regional oxygen saturation of migraneurs shows a smaller decrease in both sides compared with healthy subjects [33].

4. METHOD

4.1 Experimental Procedure

Six subjects diagnosed with migraine without aura (six females) according to IHS criteria and six healthy subjects (four males, two females) joined the study. Migraine subjects were not using prophylactic drugs and did not experienced any migraine attack at least three days prior to experiment. During the experiment, subjects were positioned in supine position and performed breath holding task for four times. Procedure of the experiment is normal breathing for 90 seconds and after exhaling air holding breath for 30 seconds.

4.2 fNIRS Data Collection

fNIRS system NIROXCOPE 201 developed at the Biophotonics Laboratory[1] is used during experiment. fNIRS system is composed of a flexible probe placed on the subject's forehead, NIROXCOPE 201 data acquisition unit, data gathering and recording computer.

Probe has four light emitting diodes (Epitex, L4*730/4*805/4*850-40Q96-I) which emit light at multiple wavelengths of 730 nm, 805 nm and 850 nm in the near infrared region and ten photodetectors (TI-Burr Brown, OPT101). Emitted light from diodes pass through the tissue and undergoes scattering, absorption or reflection. Referencing to the Figure 3.1 in Chapter 3, at 805 nm deoxygenated hemoglobin (Hb) and oxygenated hemoglobin (HbO_2) equally absorb light and it is accepted as isobestic point. Concentrations of Hb and HbO_2 can be measured approximately from the fact that near infrared light at 703 nm is highly absorbed by Hb and 850 nm light is mostly absorbed by HbO_2. The intensity of reflected light from tissue is detected by

[1] www.bme.boun.edu.tr/biophotonics

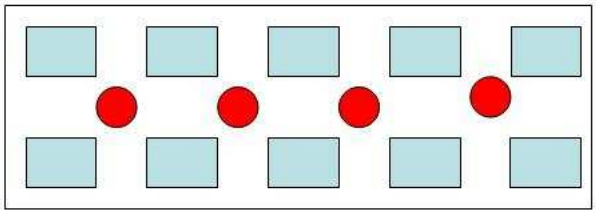

Figure 4.1 Niroxcope 201 probe: Source-detector locations

photodetectors. Four non-overlapping quadruples of photodetectors are obtained by multiplexing time and wavelength. Detectors are located equidistant to the each diode lying at the center of each quadrant. The source detector distance is 2.5 cm enabling penetration of light nearly 1.5 cm of the adult cortex. Schematic diagram of probe is shown in Figure 4.1.

4.3 Data Preprocessing

Collection and preprocessing of data is very important in system identification. Outliers and aliasing effects should be eliminated not to distort the output. Eliminating fluctuations in the heart rate due to respiration, blood pressure regulation and arterial pulse which reveal themselves on certain frequencies, is avoided, since this study aims exactly investigating the frequency responses. Observing effects of these signals is preferred on the frequency domain data. Outlier elimination is performed with a fourth degree Butterworth filter having a cutoff frequency at 0.2 Hz.

4.4 System Identification and Modeling

System is an object in which variables of different kinds interact and produce observable signals. Observable signals are called output and the external stimuli are called input. The derivation of a relevant system description from observed data is termed as system identification and the resultant system description a model. Mod-

eling and identification methods are needed for the interpretation of observations and measurements obtained from some system of study. Models present a relation between the variables of a system. Depending on the complexity of this relation and the purpose of the model, classification of models is performed. Depending on the model class, different approaches to system identification is adopted. Linear systems have a particular significance in the comparison of models, since both modeling and identification presume linear, proportional relationships to exist between variables.

Nonlinear systems can be modeled by linear time-invariant approximations. System identification is an example for this type of approximations and it is possible to estimate a linear model without considering the fact that the input and output measurements come from a nonlinear system. Since linear time-invariant models minimize a mean square error criterion, they are assumed as optimal [34].

The System Identification Procedure

Identification of a system involves four main steps:

1. *Acquisition of a data set:* Since system identification constructs a mathematical model from input and output values in a time interval which are collected from an experimental setup, obtained data should fulfill the prerequisites of identification method. Choice of input becomes very important at the point of excitation of system. Ljung ([35]) and Johansson ([36]) present hints and guidelines for the appropriate design of experiments and the selection of input.

2. *Selection of a model or a model structure:* A suitable model among candidates is selected according to the representation capability of the model of the system. a priori knowledge about the system dynamics or the physical properties of the system give advantage in the prediction of the suitable model.

3. *Parameter Estimation:* Identification part arises and several parameter estimation methods are applied on a set of candidate models

4. *Model Validation:* After finding a particular model, this model is tested according

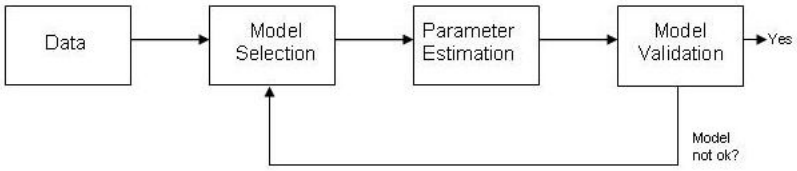

Figure 4.2 Algorithm for the system identification

to a chosen criterion. Relation between the model and the measured signal, prediction capability of future outputs and the consistency of the model with the purpose are tested by model validation processes.

All aspects of system identification will not be discussed. In this study, ARX modeling is used as a system identification tool to model brain hemodynamic response. One of the reason applying ARX model is no a priori information about the system is required and its simplicity in application. Section 4.5 discusses ARX model as a linear parametric identification technique and modeling schemes associated with it.

4.5 ARX Model

ARX model describes the relationship between output signal, input signal and noise term in a form of difference equations. Value of the output signal at time t is equal to the summation of determined number of past values of input and output signal and noise term. Difference equation is in the form:

$$y(t)+a_1y(t-1)+...+a_{na}y(t-n_a) = b_1u(t-n_k)+...+b_{nb}u(t-n_k-n_b+1)+e(t) \quad (4.1)$$

where y(t) represents the output at time t, u(t) represents the input at time t, n_a is the number of a parameters, n_b is the number of b parameters, n_k is the number of samples before the input affects output of the system (the delay), and e(t) is the white-noise disturbance. n_a and n_b are orders of ARX model. Transfer function representation of

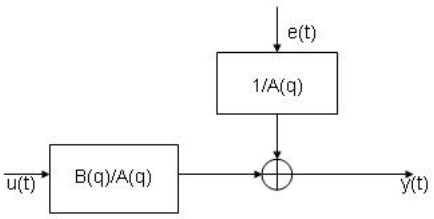

Figure 4.3 Block diagram of ARX model

the Equation 4.1 is[2] :

$$y(t) = G(q)u(t) + H(q)e(t) \tag{4.2}$$

where $A(q) = 1 + a_1q^{-1} + ... + a_{na}q^{-na}$ and $B(q) = b_1q^{-1} + ... + a_{nb}q^{-nb}$. G(q) and H(q) is therefore;

$$G(q) = \frac{B(q)}{A(q)} = \frac{b_1q^{-1} + ... + a_{nb}q^{-nb}}{1 + a_1q^{-1} + ... + a_{na}q^{-na}} \tag{4.3}$$

$$H(q) = \frac{1}{A(q)} = \frac{1}{1 + a_1q^{-1} + ... + a_{na}q^{-na}} \tag{4.4}$$

The calculation of output signal in Equation 4.1 from past data depends on the parameters in the vector $\theta = [a_1...a_nb_1....b_n]$ and $\phi(t) = [-y(t-1).... - y(t-n)u(t-1)....u(t-m)]$ which can be represented as:

$$\hat{y}(t) = \phi^T(t)\theta \tag{4.5}$$

There are various methods for estimation of parameters. In this study linear least square method is used for the calculation of parameters since it can be used even if there is no a priori information available. Linear least square method aims to determine the optimal values of the estimated parameters by minimizing the sum of the squared errors between the predicted output and the observations [35]:

$$V_N = \frac{1}{N}\sum_{t=1}^{N}(y(t) - \hat{y}(t))^2 = \frac{1}{N}\sum_{t=1}^{N}(y(t) - \phi^T(t)\theta)^2 \tag{4.6}$$

[2] $q^{-1}u(t) = u(t-1)$

The least square solution of θ that minimizes the squared error or loss function V_N can be found by taking the derivative of V_N with respect to θ;

$$\frac{d}{d\theta}V_N = \frac{2}{N}\sum_{t=1}^{N}\phi(t)(y(t) - \phi^T(t)\theta) = 0 \tag{4.7}$$

$$\sum_{t=1}^{N}\phi(t)y(t) = \sum_{t=1}^{N}\phi(t)\phi^T(t)\theta \tag{4.8}$$

$$\theta = \left[\sum_{t=1}^{N}\phi(t)\phi^T(t)\right]^{-1}\sum_{t=1}^{N}\phi(t)y(t) \tag{4.9}$$

where N is the number of samples. Linear least squares method has some attractive features for purposes of identification. Least square estimates can be obtained by matrix algebra and properties of solution of least squares estimation can be analyzed according to statistical criteria [36]. For least square estimate to be consistent i.e. the estimate $\hat{\theta}$ converges to the true value θ two conditions should be satisfied. First, $\sum_{t=1}^{N}\phi(t)\phi^T(t)$ is non-singular that is its inverse exists. Second, noise component of the model is a sequence of independent random variables with a zero mean values and input signal is uncorrelated with the noise component [35].

By introducing least square method, system identification is reduced to determination of model orders and model parameters in the sense that optimal fitting of output predicted from the model and measured output. Linear least squares method finds model parameters by minimizing the error between computed output and measured one. However, for the solution of Equation 4.6, determination of model orders is needed. As the correct model order is not known a priori, several different model orders can be implemented and according to some error criteria one of them can be selected. This process is known as model validation. Many tools are presented for model validation where three of them are used in this study:

- **Residual tests:**

  Differences between the observed output and the estimated output are called residuals:

$$\varepsilon(t) = y(t) - \hat{y}(t) \tag{4.10}$$

If the model is correct, residuals should be uncorrelated to inputs and outputs. The auto-correlation function of the residuals and the cross-correlation between residuals and the input data are computed. A good model has the residual autocorrelation function inside the model confidence interval indicating that the residuals are uncorrelated. If residuals are correlated with past inputs, this indicates there is a part of output signal originates from the past input and is not properly described by the model.

- **Model Fit:**

  Minimum fit error between the simulated output and measured output indicates a good model. The command 'compare' in Matlab program computes the model fit as the percentage of the output variation:

$$fit = 100\left(1 - \frac{\parallel \hat{y}(t) - y(t) \parallel}{\parallel y(t) - \overline{y}(t) \parallel}\right) \tag{4.11}$$

  where $\overline{y}(t)$ denotes mean of the measured output over the time interval. Since error is subtracted from 1, the largest model fit is suitable.

- **Cross validation**

  Cross validation method is performed with another set of output signal which is not used in prediction of output. Validation data is generated by splitting the measured data in two parts. Parameters that minimizes the criterion of the model predicted from estimation data set $Z_{est}^{N_1}$ are used for the evaluation of model from the validation data set $Z_{val}^{N_2}$.

  An attractive feature of cross-validation approach is the fact that regardless of the probabilistic arguments and without any assumptions about the system, minimization of loss function makes sense.

Since output of a system in ARX modeling is represented by two components: deterministic (input) and stochastic (white noise) signals, it is widely used in noise free processes. One example of the ARX modeling in biomedical signal processing is the analysis of EEG and fMRI signals in especially detection of evoked potentials [37, 38, 39]. In these studies, it has been hypothesized that measured signal is composed

of useful signal and noise contribution which is formulated as background activity. By using ARX modeling as a filtering procedure useful signal is extracted from measured signal.

In this present study, regarding the previous studies on parametric identification of biomedical signals, three ARX modeling schemes are followed which differ from each other in the selection of inputs. It is important to note that, time-domain analysis of fNIRS data was performed by using Gaussian functions in modeling brain hemodynamic response of migraine and normal subjects previously [40]. In this previous study, it is successfully shown that brain hemodynamic responses of migraine subjects in time domain differs from normal ones in signal amplitude and time to peak parameters. Different from that study, differences in frequency data of brain hemodynamic responses of two experiment groups are investigated.

4.5.1 Determining Input and Output Signals of the ARX Model

In the first two modeling schemes, tissue oxygenation of the brain is supposed as a system and input signal is constituted from breath holding protocol. It is assumed that input signal takes zero value during normal breathing and one during breath hold. [Hb] data obtained from 16 detectors of fNIRS for each one of the 12 subjects is considered as output signal. After preprocessing, [Hb] data is partitioned in four parts each corresponding to one breath hold. Each fraction of [Hb] data lasts 100 seconds having 30 seconds of breath holding episodes. Output signal is downsampled[3] with a factor of three and input signal is generated synthetically for each of the fraction according to start and end of breath hold i.e. during breath hold signal takes value of one. Figure 4.4 shows input and output signals before partitioning into breath holds.

In the third modeling scheme, rather than using square wave as input, a reference signal of [Hb] data is used. The input signal is selected as the average of a sufficient number of detectors which provides mean behavior of the response for the considered

[3]Matlab command *resample* is used

a

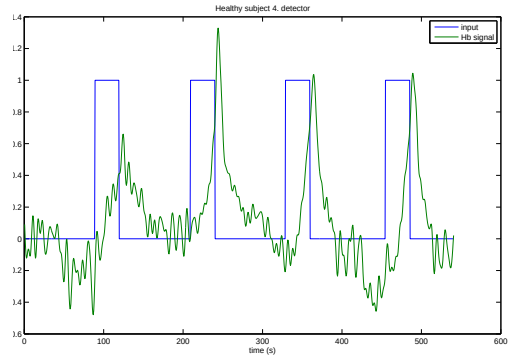

b

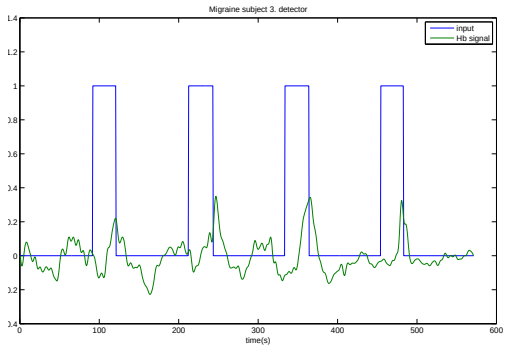

Figure 4.4 Input and output signals of the ARX models. (a) Hb signal taken from fourth detector of fNIRS from a normal subject and corresponding hypothetical input signal and (b) Hb signal taken from third detector of fNIRS from a migraine subject and corresponding hypothetical input signal

subject. By this way, it is aimed to eliminate background activity component and focus on the response to breath holding task.

After decision of the input and output signals for the ARX models, three modeling schemes are followed. One scheme is building ARX model for each breath hold episode of each detector for every subject. After finding most suitable ARX models for each signal, frequency response of the predicted model is found and analyzed. For the second modeling scheme, data from the 16 detectors and 4 breath hold episodes are averaged for each subject. Optimal ARX models are generated for the averaged data and analysis of the coefficients of the ARX models is performed.For the third modeling scheme, ARX modeling is used as a filtering preocedure to eliminate white noise from measured signal. ARX models are built for each detector and power spectrum of

filtered signal is calculated.

4.5.2 ARX Modeling Scheme-1

The block diagram in Figure 4.5 illustrates the ARX modeling scheme 1 for each subject. For each 6 healthy and 6 migraine subject, all possible causal ARX models with orders m and n corresponding to number of past outputs and inputs respectively, ranging from 10 to 20 utilizing square wave as input and [Hb] data as output are considered (16x4x10x10=6400 models). The reason for using relative high orders is the 'difficulty' of modeling of the [Hb] data. Lower orders fail to model data. Interpretation of using high orders is predicting the output value at time t requires more past values in both output and input.

Predicted models are cross validated with the [Hb] data of the succeeding breath hold. The first data set is used to estimate the model parameters and the succeeding data set is used to calculate the normalized sum of the squares of the difference between validation data output and the model output (loss function). For the cross-validation test, the command 'arxstruc' in Matlab program is used which estimates an ARX model for each model order from estimation data set. After calculation of loss functions of each model with validation data set, model fits between predicted output of each model and measured data are computed according to the Equation 4.11. Models with minimum loss functions and maximum model fits are accepted as the optimal model. Frequency response of optimal models are calculated. This procedure is followed for each of the breath hold episode, detector and subject.

4.5.3 ARX Modeling Scheme-2

Modeling scheme 2 differs from 1 in the output signal. In this scheme, instead of building model for each 16 detector recording, detector recordings are averaged and 4 models are constructed for each subject. This scheme surveys the diversity of the

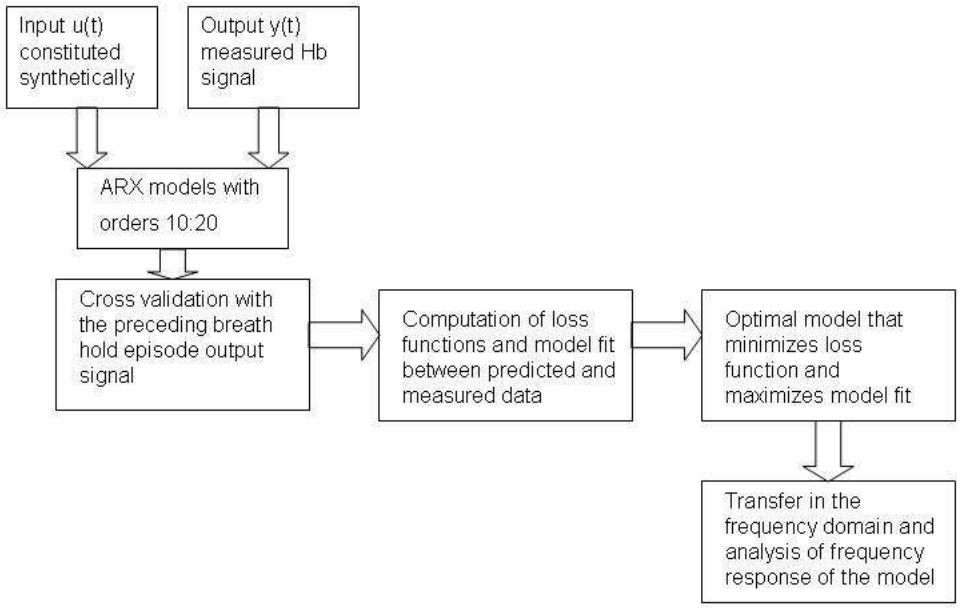

Figure 4.5 Block diagram of the ARX modeling scheme 1

parameters used in ARX modeling.

As similar to ARX modeling scheme 1, for each 6 healthy and 6 migraine subject all possible causal ARX models with orders m and n corresponding to number of past outputs and inputs respectively, ranging from 10 to 20 utilizing square wave as input and [Hb] data as output are considered(4x10x10=400 models). The third term of the model order, delay term d is determined by trial and error method. In addition to loss function and model fit criterion, residual check is also performed to analyze the success of models.

Residuals are the differences between predicted output and measured output. It is assumed that model which has residuals exhibiting white noise pattern with zero mean and variance λ and independent from past inputs is successful in predicting the measured data. The autocorrelation function of the residuals carry information about whether the residuals can be regarded as white. To investigate the independency between the residuals and past inputs, cross correlation between input and output can be checked. If the residuals are not uncorrelated with input, this means model could not picked up a part of output which originates from past input. The confidence

interval for the auto correlation of residuals and cross correlation corresponds to the range of residual values with a specific probability of being statistically insignificant for the system.

In ARX modeling scheme-2 residual check is performed both for estimation and validation data. Models are forced to have minimum 90 % model fit with the estimation data. However, minimizing loss functions and pass of the residual check is also performed.

4.5.4 ARX Modeling Scheme-3

It is intended to decompose the measured fNIRS signal into two contributions and extract the uncorrupted [Hb] signal.

1. The first contribution is the 'useful signal' which is the cerebrovascular response of brain to breath holding task. In Equation 4.2 the input signal is filtered with a transfer function obtained from the model (Fig. 4.6). The poles and zeros of this transfer function are determined by using a proper identification algorithm. In the model $s(k)$ denotes the filtered average reference signal.

2. The second contribution is the background activity of fNIRS which can be modeled as the response of an auto-regressive filter driven by a white noise. In some cases background activity hinders the main response of vessels to breath holding. To avoid this problem, it is assumed that filtered version of white noise corresponds to the background activity.

The block diagram of the processing procedure is depicted in Figure 4.6. In this modeling scheme it is intended to model existent background activity of cerebrovascular system i.e. concentration changes of [Hb] in absence of a stimulus, as an autoregressive (AR) process driven by white noise [39]. To test this hypothesis, we take measurements from four healthy subjects while subjects are in supine position and normal breathing.

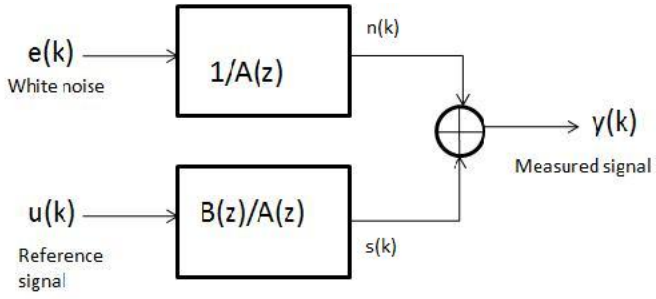

Figure 4.6 Block diagram of the ARX modeling scheme 3: $s(k)$ is the filtered version of average reference signal, $n(k)$ denotes modeled background activity

Duration of measurements is adjusted as same in breath holding procedure. Normal breathing data is modeled with autoregressive modeling which has a equation in the form:

$$y(t) = -a_1 y(t-1) - ... - a_{na} y(t-n_a) + e(t) \tag{4.12}$$

where y(t) represents the output at time t, n_a is the number of a parameters, e(t) is the white-noise disturbance. n_a is the order of AR model.

Measured [Hb] data stands for the output of AR model where AR models are built in a detector based manner (Fig. 4.7). All possible casual AR models with order ranging from 1 to 20 are used to fit the background activity measurements. Optimal order for AR models are chosen regarding the whiteness of residuals and minimum loss function criterion.

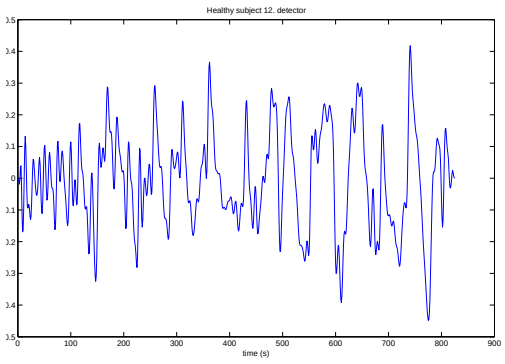

Figure 4.7 Measured [Hb] data from 12. detector during normal breathing

In ARX model case, for the model order m which denotes the AR process, result of AR model is considered. Since the identification of ARX model is utilized from a reference input which has a similar pattern with the output signal, lower orders of n are preferred ranging from 1 to 8. Validation of ARX models are performed regarding the whiteness of residuals and maximum model fit between predicted and measured response. In fact, assumption in this modeling scheme may not completely reflect the real case due to the linear superposition of background activity and hemodynamic response relating to breath holding.

5. RESULTS AND DISCUSSION

Results from system identification of [Hb] data show significant differences between normal and migraine subjects. Statistical significance of data is tested by two-way ANOVA. Common significance level for p is 0.05 indicating one sample mean is significantly different from the others. Throughout analysis, p value is used for the indication of significant differences between normals and migraineurs.

5.1 Results from ARX Modeling Scheme-1

ARX modeling scheme-1 estimates ARX models according to first the loss function and secondly model fit criterion. Model fit is forced to be minimum 80% to capture all measured data. Figure 5.1 depicts the comparison between modeled and measured response graphs for healthy and migraine subjects.

After building a model in time domain, frequency response analysis of the predicted model is performed in the frequency range (0, 0.2953). This frequency interval is consistent with the sampling frequency (Fs = 0.5908). Power spectrum of predicted model is plotted on the basis of 16 detectors and 4 breath holds. ANOVA test is applied at all 256 frequency points for each breath hold of each detector and frequencies which are statistically significant i.e. give $p<0.05$ in comparison of normal subjects and migraineurs, are signed. Colored demonstration of significant frequencies for each breath hold is depicted in Figure 5.2. Color bar shows corresponding colors used for frequencies in the interval (0, 0.2953). Horizontal axis of each graph shows detectors from 1 to 16 and vertical axis shows the number of significant frequencies.

In the first breath hold graph, significant frequencies from all detectors are mostly near 0.05 Hz and 0.15 Hz. Also some detectors show significant frequencies near 0.15 Hz and above 0.25 Hz. In the second breath hold graph, number of significant

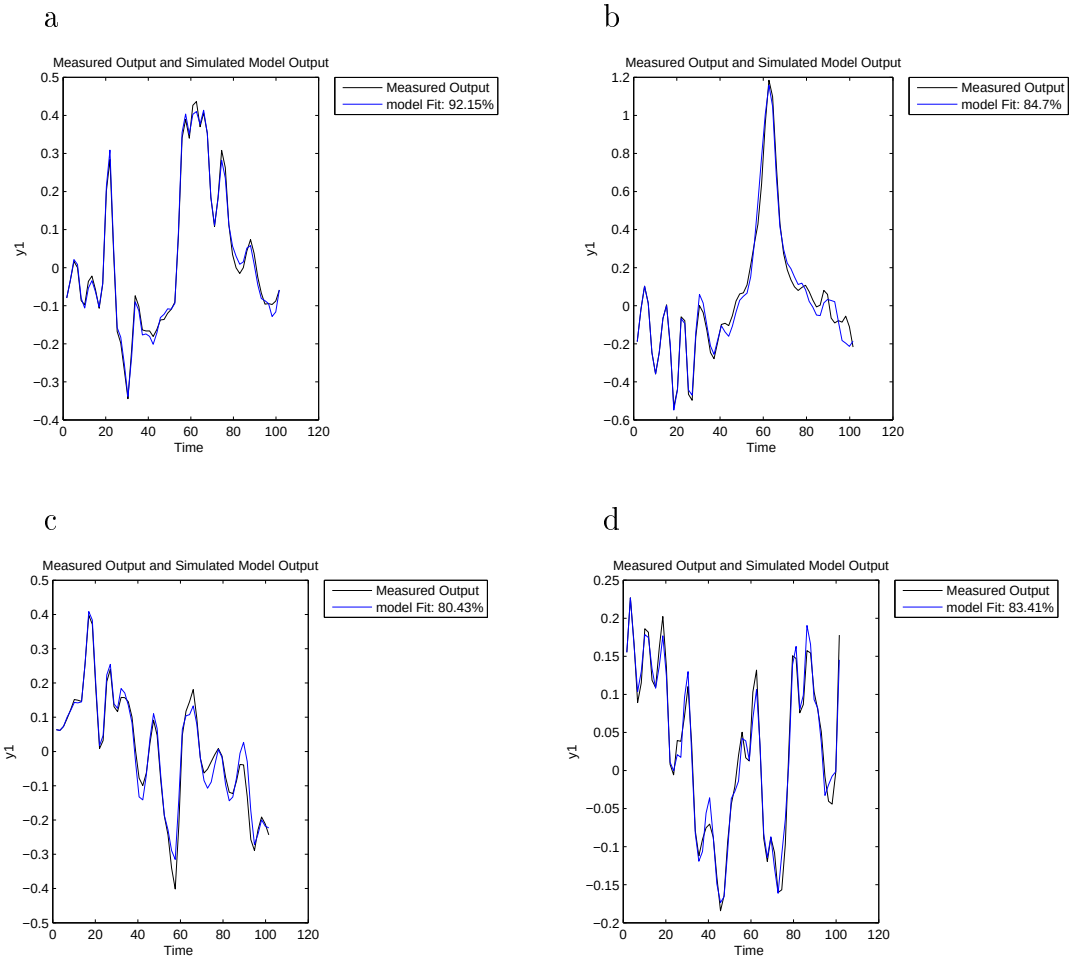

Figure 5.1 Model fit plots of [Hb] data taken from 14. detector during first (a,c) and second (b,d) breathholds for healthy (a,b) and migraine (c,d) subjects

frequencies is larger indicating estimated power spectrum of normals differs more from estimated power spectrum of migraineurs. Significant frequencies are located mostly below 0.05 and around 0.1, 0.2 and above 0.25 Hz. On the contrary to first breath hold, second breath hold gives more significant frequencies near 0.1 Hz. Third breath hold shows lesser low frequencies (near and below 0.05) whereas more high frequencies (above 0.15 Hz). Fourth breath hold shows all type of frequencies. Common point for all breath holds is nearly equal number of significant frequencies below 0.05 Hz for all detectors. From these graphs, it is interesting to note that frequencies between 0.1 Hz and 0.2 Hz are not mostly significant for first breath hold where as they appear mostly in succeeding breath holds. In addition first breath hold is less 'colored' denoting power spectrum of normals and migraineurs are close, whereas succeeding breath holds are more 'colored'. Significant frequencies between 0.1 and 0.2 are mostly observed in second and third breath holds.

After applying ANOVA test on the estimated power spectrum of normals and migraneurs on the basis of each detector, for further investigation of significant frequencies, power spectrums obtained from 16 detectors are averaged for each subject and ANOVA test is applied on each frequency point for four breath holds to find significant frequencies. For each breath hold, each detector recording of all subjects is averaged over subjects. Secondly, computed data is averaged over subjects. Thus, localization assumption for subjects is avoided. On the averaged signal, values corresponding to significant frequencies are summed for healthy and migraine subjects. Results are shown in Table 5.1.

At first glance to Table 5.1, one can observe that sum of averaged estimated power spectrum of migraine subjects is always smaller than the healthy ones for every frequency interval. Frequencies below 0.02 Hz are significant frequencies for each breath hold. Power spectrum corresponds to these frequency is very large. There are three significant frequency bands for first breath hold episode: below 0.06, 0.12 and 0.27 Hz. Except the first breath hold episode, all episodes have significant frequencies around 0.1-0.15 Hz. All episodes show significant frequencies above 0.2 Hz. From this table, it can be concluded that migraine subjects have a depressed estimated power spectrum

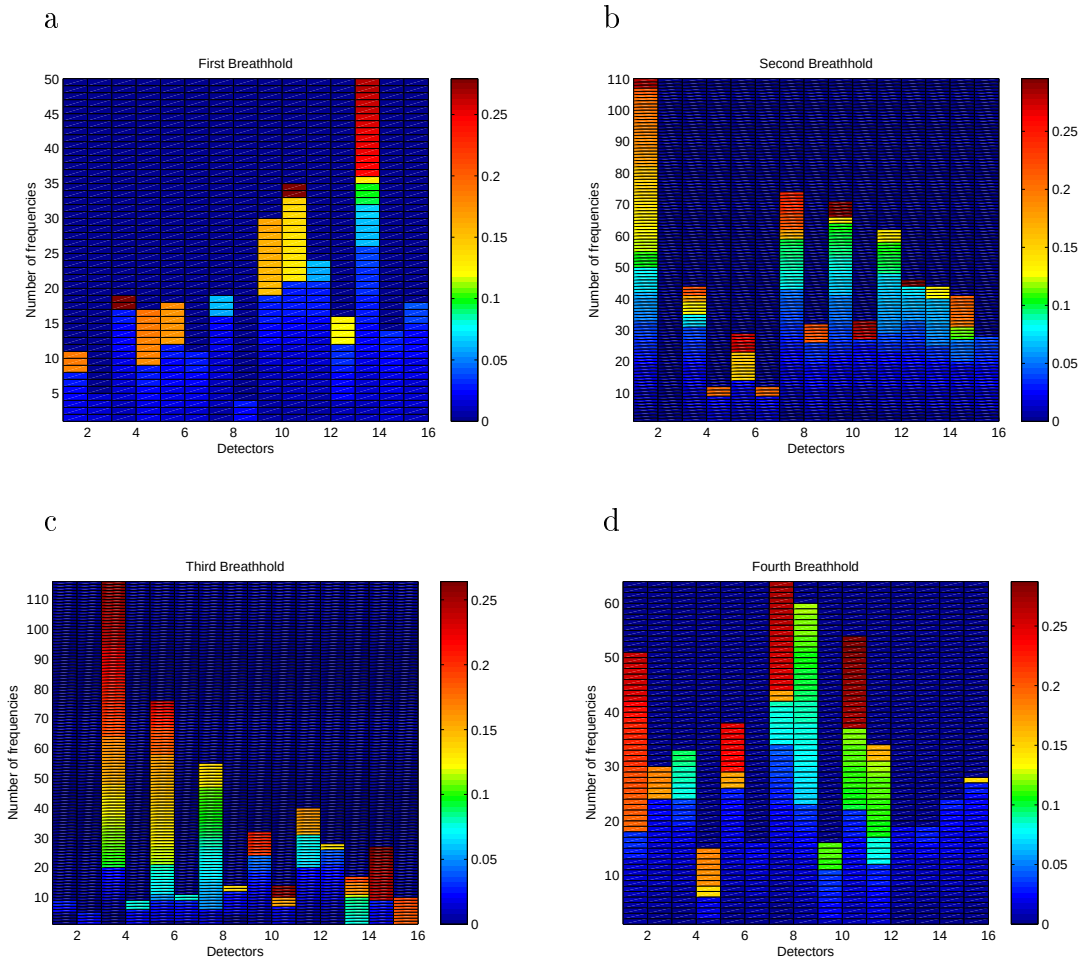

Figure 5.2 Demonstration of statistically significant frequencies based on 16 detector recordings for each breath hold

Table 5.1
Significant frequency intervals and corresponding sum of estimated power spectrums

	Significant Frequency Interval		**Sum of Power Spectrum**	
	Start	**End**	**Normal**	**Migraine**
First Breath Hold	0.0093	0.0336	48.5068	10.6591
	0.0521	0.0649	13.7120	7.1704
	0.1251	0.1297	3.9079	2.6321
	0.2711	0.2769	0.0334	0.0341
Second Breath Hold	0.0012	0.0811	89.9575	23.6441
	0.1228	0.1378	9.4806	5.2800
	0.1656	0.1749	4.7305	2.8850
	0.1981	0.2074	1.5195	0.8409
	0.2398	0.2491	0.3001	0.1457
	0.2734	0.2826	0.0460	0.0252
Third Breath Hold	0.0012	0.0278	29.8673	9.0230
	0.0985	0.1043	3.3643	2.7047
	0.1135	0.1205	7.7959	6.0922
	0.1332	0.1367	2.2281	1.7029
	0.2097	0.2224	1.4926	0.7990
	0.2398	0.2491	0.3223	0.1570
Fourth Breath Hold	0.0012	0.0405	48.1610	11.9288
	0.0788	0.0846	3.4607	2.2513
	0.0973	0.1043	4.4311	2.4449
	0.1992	0.2027	1.1038	0.4277
	0.2491	0.2514	0.0612	0.0345

response. Also frequency ranges found from averaged estimated power spectrum are consistent with ones in Figure 5.2.

Figure 5.3 shows the average power spectrums of healthy and migraine subjects. During all breath hold episodes, average power spectrum of normal subjects reach a peak at a frequency below 0.05 Hz. However, amplitude of power spectrum of migraine subjects are at same frequencies is very low relative to normals. Peak at spectrum below 0.05 Hz is due to rise in [Hb] amplitude in time domain. In normal subjects during breath hold episodes [Hb] data resembles triangular wave with a period of minimum 30 seconds (Fig. 5.1). Frequency domain representation of triangular wave is a sinc function centered at nearly 0.033, depending on the location of peak. Since migraine subjects do not show a significant [Hb] increase during breath hold, this peak can not be observed as dominant relative to healthy case.

Spectral analysis of modeled [Hb] signal of migraine and healthy subjects gives some clues in the vasoconstrictive character of cerebrovascular system of migraineurs. A detailed analysis of Table 5.1 to determine the frequencies which are significant in all breath holds i.e. intersection of frequencies between all breath holds, deduces that at very low frequency(VLF): 0.01-0.03 Hz, low frequency(LF): 0.13 Hz and high frequency(HF): 0.25 Hz are mutual frequencies for four breath holds (Fig. 5.4). For both healthy and migraine subjects, power spectrum of [Hb] signal takes its maximum values at VLF whereas energy of migrainuers response is approximately five times even nine times for second breath hold, smaller than healthy subjects' response. Maximal character of power spectrum in VLFs for both subject groups is related to the peak of time domain [Hb] signal at the end of the 30 seconds breath holding period. Amplitude difference in power spectrum may be an evident for the lack of vasoregulation in migraneurs which is shown in other studies [31, 32, 41]. Breath holding task requires the vasodilation of cerebral vessels by increasing the arterial partial pressure of carbon dioxide from its normal level and decreasing the arterial partial pressure of oxygen [42]. Increased partial pressure of carbon dioxide leads vasodilation [43]. At VLF where response to breath holding task dominates, vasoreactivity behavior of migraineurs is found very different from normals meaning an impairment in the autoregulation.

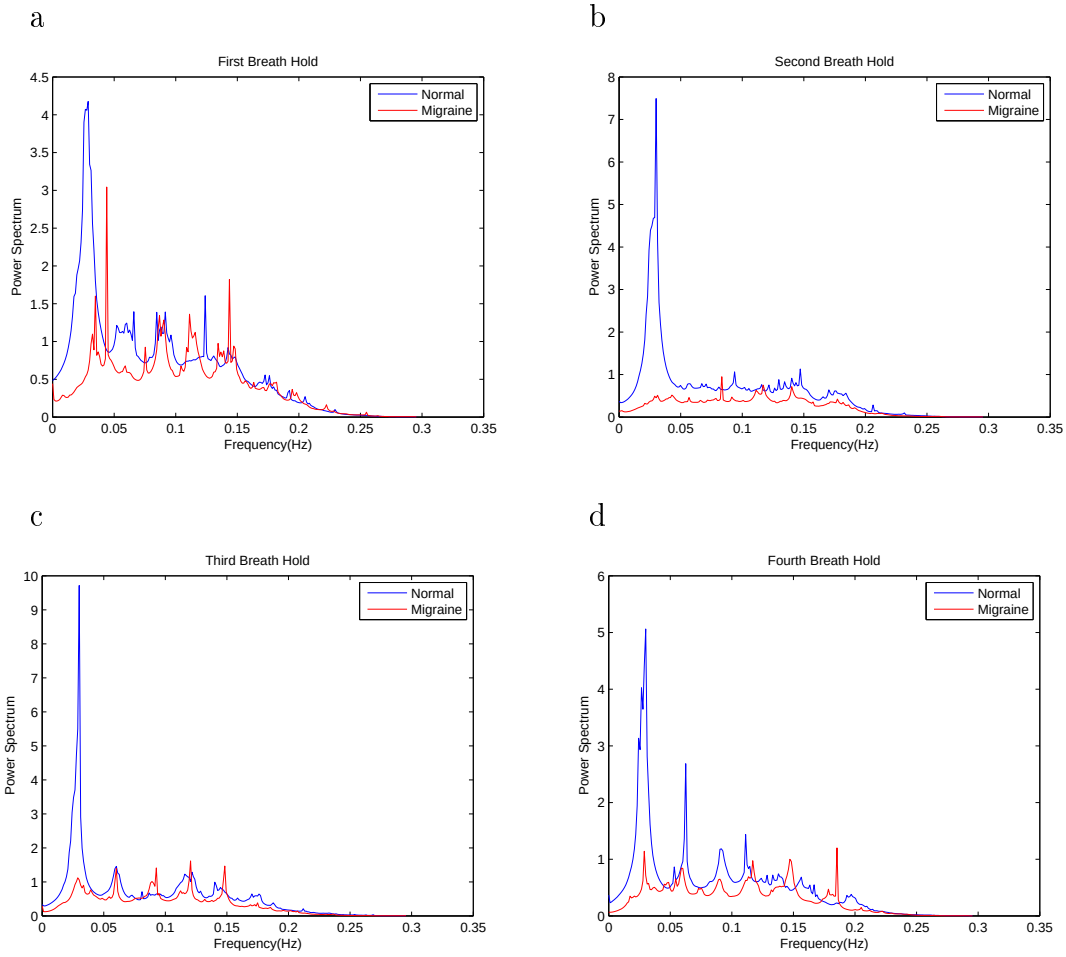

Figure 5.3 Average power spectrum from healthy and migraine Patients

Spectral analysis of cerebrovascular dynamics and metabolism have been studied widely with different techniques to investigate the oscillations. However, there has been no agreement on the frequency of oscillations [44]. In our study we found that around 0.13 Hz energy of estimated [Hb] signal of migraneurs shows a statistically significant diversity from healthy subjects with a 1.5 fold decrease. Although it is not clear, some studies have shown that 0.13 can be a low frequency oscillation which stems from the vascular or metabolic regulations [45, 46].

Although it can not seen from Figure 5.3, statistical analysis on frequency spectrum has shown a significant difference at 0.25 Hz in the estimated power spectrum of migraine and healthy subjects. Oscillations higher than 0.2 and 0.3 Hz are attributed as respiratory frequency [47]. Similar to VLF and LF, energy estimates of migraineurs

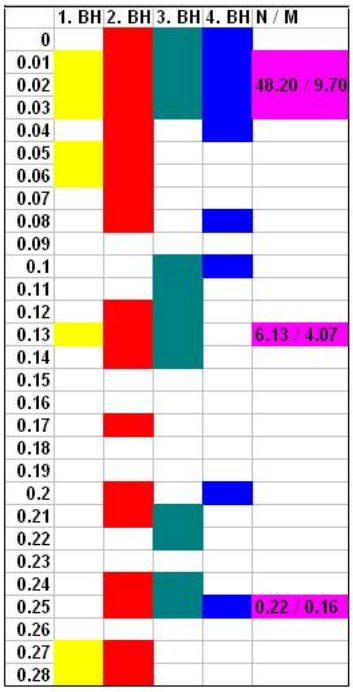

Figure 5.4 Overlapping frequencies in four breath holds. Pink colored cells are the mutual frequencies where at least three breath holds show significant differences. The energy of the each overlapping interval is denoted on the left for normals and migraneurs

are found smaller relative to healthy subjects.

5.2 Results from ARX Modeling Scheme-2

ARX modeling scheme-2 estimates ARX models from averaged [Hb] data over 16 detectors recordings for each healthy and normal subjects. Different from scheme-1 model fit between estimated and measured data is forced to 90%. Candidate models that have small loss functions and 90% model fit are selected according to the residual check. Residual check is performed on both estimation and validation data. Estimated models which have an autocorrelation sequence of residuals and a cross correlation sequence of residual and input lay in the confidence region, are selected as optimal models. Figure 5.5 depicts residual plot of a selected model.

Table 5.2 shows the required model orders to model averaged [Hb] data of healthy and migraine subjects. All models fulfill the loss function and model fit crite-

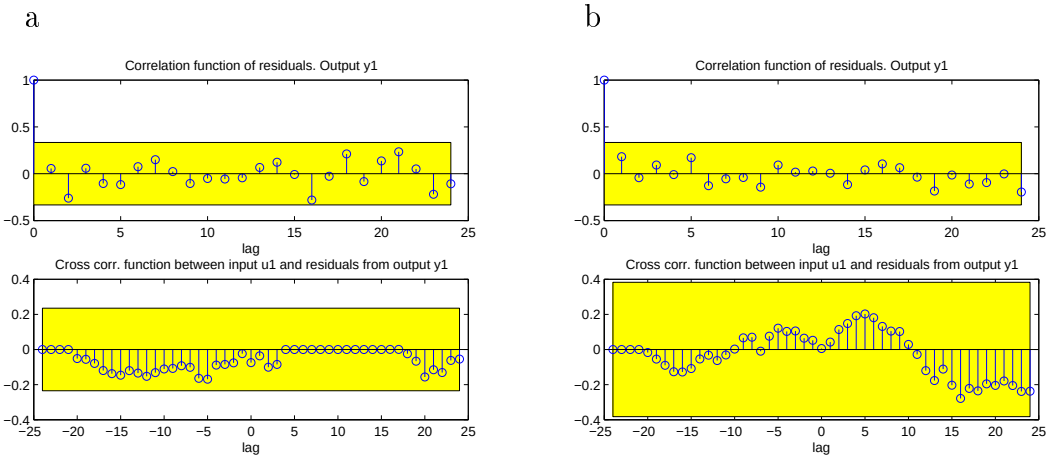

Figure 5.5 Residual check performed on (a) estimation data and (b) validation data

rion, also they satisfy residual check.

Table 5.2 shows that in four breath hold episodes, although a statistical difference can not be elicited for all breath holds, averaged [Hb] data of migraine subjects requires higher model orders and in some cases ARX model fails in finding successful models when same input signal is applied.

5.3 Results from ARX Modeling Scheme-3

First of all, background activity is modeled as AR process by taking normal breathing measurements from healthy subjects. Orders from 1 to 5 has been found satisfying which successfully model all data from four subjects. Therefore AR order which will be applied to ARX modeling is determined as [1:5].

The ARX modeling procedure in Section 4.5.4 is applied to the whole [Hb] breath holding signals obtained from subjects. Signal u(k) is obtained by averaging detectors which reflect the behavior of response. All 16 detectors are not used not to decompose the pattern of reference input. For each subject approximately 6 detectors are accounted for modeling. Table 5.3 shows the averaged model orders for each subject

Table 5.2
Orders of selected models for healthy and migraine subjects for each breath hold episodes

First Breathhold									
Normal	**na**	**nb**	**nk(delay)**	**Total**	**Migraine**	**na**	**nb**	**nk(delay)**	**Total**
N1	20	8	5	33	**M1**	14	17	4	35
N2	10	19	5	34	**M2**	20	13	2	35
N3	20	12	0	32	**M3**	20	13	3	36
N4	20	3	5	28	**M4**	14	17	0	31
N5	14	19	1	34	**M5**	20	14	2	36
N6	20	9	4	33	**M6**	not model	not model	not model	
Mean	17.33	11.67	3.33	32.33	**Mean**	17.60	14.80	2.20	34.60
St Dev	4.32	6.38	2.25	2.25	**St Dev**	3.29	2.05	1.48	2.07
Second Breathhold									
Normal	**na**	**nb**	**nk(delay)**	**Total**	**Migraine**	**na**	**nb**	**nk(delay)**	**Total**
N1	19	9	5	33	**M1**	not model	not model	not model	
N2	12	17	4	33	**M2**	20	14	0	34
N3	19	13	0	32	**M3**	20	18	1	39
N4	20	7	5	32	**M4**	11	20	5	36
N5	16	12	5	33	**M5**	19	15	2	36
N6	12	16	5	33	**M6**	20	6	5	31
Mean	16.33	12.33	4.00	32.67	**Mean**	18.00	14.60	2.60	35.20
St Dev	3.61	3.88	2.00	0.52	**St Dev**	3.94	5.37	2.30	2.95
Third Breathhold									
Normal	**na**	**nb**	**nk(delay)**	**Total**	**Migraine**	**na**	**nb**	**nk(delay)**	**Total**
N1	15	13	5	33	**M1**	18	12	4	34
N2	18	14	5	37	**M2**	19	14	5	38
N3	20	9	5	34	**M3**	20	5	5	30
N4	7	20	5	32	**M4**	13	19	5	37
N5	13	10	5	28	**M5**	17	12	4	33
N6	19	15	5	39	**M6**	11	20	3	34
Mean	15.33	13.50	5.00	33.83	**Mean**	16.33	13.67	4.33	34.33
St Dev	4.84	3.94	0.00	3.87	**St Dev**	3.56	5.47	0.82	2.88
Fourth Breathhold									
Normal	**na**	**nb**	**nk(delay)**	**Total**	**Migraine**	**na**	**nb**	**nk(delay)**	**Total**
N1	18	12	4	36	**M1**	19	13	5	37
N2	19	14	5	37	**M2**	12	20	5	37
N3	20	5	5	31	**M3**	17	20	1	34
N4	13	19	5	26	**M4**	20	7	4	35
N5	17	12	4	33	**M5**	19	19	0	38
N6	11	20	3	34	**M6**	15	18	1	35
Mean	16.33	13.67	4.33	32.83	**Mean**	17.00	16.17	2.67	36.00
St Dev	3.56	5.47	0.82	3.97	**St Dev**	3.03	5.19	2.25	1.55

where model orders are denoted as mean(stdev) over selected detectors. It can be seen that model orders required for modeling scheme-3 are very low comparing to orher modeling schemes due to the difference in input signals. In modeling scheme-3, models predict the output signal from a similar signal whereas in other modeling schemes input is square wave.

Table 5.3
Averaged orders of models for healthy and migraine subjects

Normals	**na**	**nb**	**Migraine**	**na**	**nb**
N1	1.00	3.80 (0.84)	**M1**	1.40 (0,55)	3.20 (1,79)
N2	1.00	3.25 (1.39)	**M2**	1.80 (1,79)	4.00 (1,87)
N3	1.60 (0,34)	3.60 (1.67)	**M3**	1.17 (0,41)	5.33 (3,67)
N4	1.00	2.40 (0.55)	**M4**	1.00	4.00 (1,15)
N5	1.38 (0,52)	2.63 (1.06)	**M5**	1.00	3.60 (0,89)
N6	1.00	2.40 (0.55)	**M6**	1.00	3.67 (2,08)
Mean	1.16 (0,26)	3.01 (0.62)	**Mean**	1.23 (0,32)	3.97 (0,73)

Figure 5.6 shows examples of the filtered responses acquired from healthy and migraine subjects. As seen from figure, parametric ARX modeling could discard the unexpected fluctuations and abruptness in the measured signal due to movement or motion of subjects during data collection. Thus, a significant improvement is elicited from measured signal to filtered signal. Modeled background activity is depicted in Figure 5.7. Signal n(k) is found by subtracting filtered response from measured signal. Comparison of the signal in Figure 5.7 with measured normal breathing signal in Figure 4.7 which shows the normal breathing measurements, demonstrates how ARX model is successful in filtering the measured signal.

Before going on the time domain analysis of filtered responses, frequency characteristics of background activity of migraine and normal subjects is analyzed. As shown in Section 5.1, frequency response of migraineurs during breath holding task is significantly different from healthy subjects. We searched whether this difference is also valid for normal activity of neurovascular system. Simulated breath holding [Hb] signal is subtracted from measured signal and power spectrum of extracted signal is

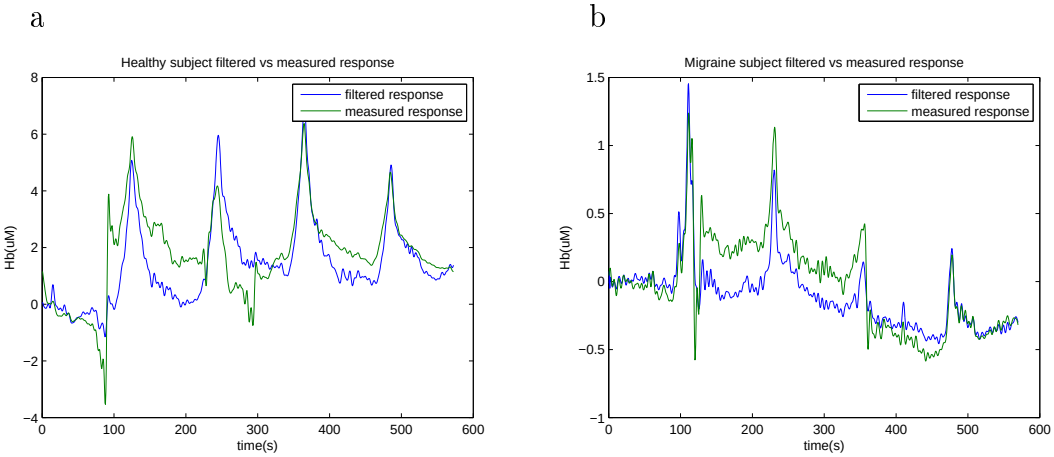

Figure 5.6 Measured and filtered responses. (a) Hb signal taken from 12. detector of fNIRS from a normal subject and corresponding filtered signal and (b) Hb signal taken from 4. detector of fNIRS from a migraine subject and corresponding filtered signal

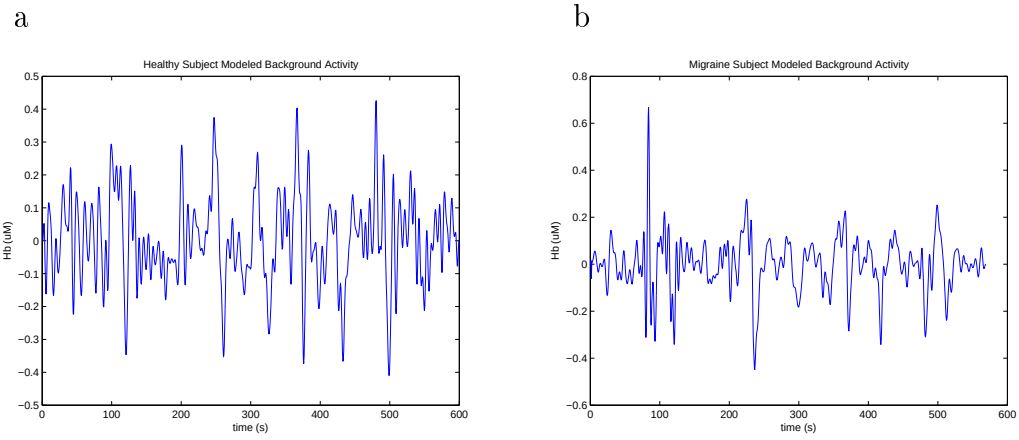

Figure 5.7 Modeled background activity for 13. detectors of normal and migraine subjects

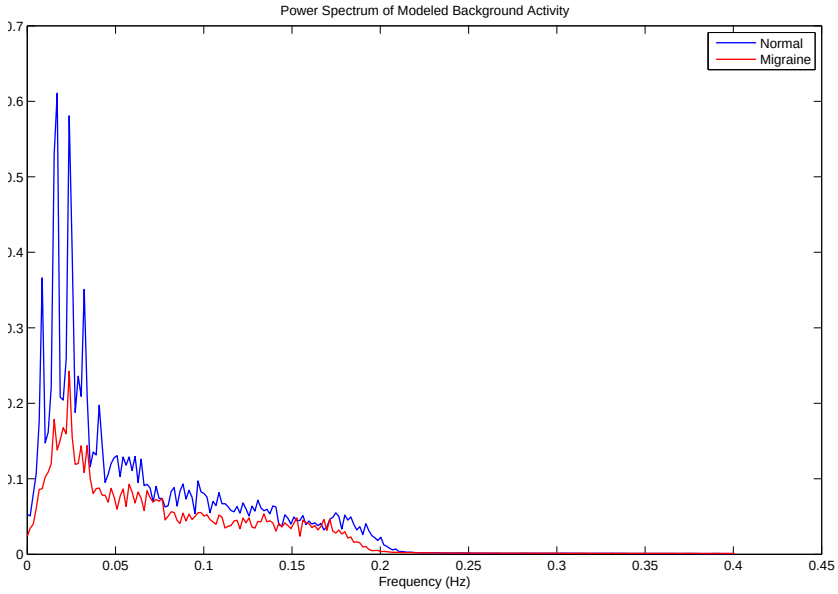

Figure 5.8 Power spectrum of modeled background activity for migraine and healthy subjects

calculated via fast Fourier transform. In order to avoid problems in Fourier transform stem from difference in length of signals, each signal length is normalized. Figure 5.8 shows power spectrum of background activity for migraine and healthy subjects.

Power spectrum graph displays depressed background activity in migraine subjects. At frequencies below 0.05Hz, healthy subjects' activity is nearly three fold of migraineurs. At frequencies higher than 0.05 Hz, this difference continues in two fold manner where magnitude of power spectrum belonging to healthy subjects is around 0.1 and migraine subjects around 0.05.

In previous section, it has been shown that frequency domain data of migraineurs significantly differ from healthy subjects in both amplitude and frequency characteristics. It is important to analyze the time domain data of the signal obtained after parametric identification, s(k), for the demonstration of difference between two groups. This analyses would show whether there exists a dissimilarity in neurovascular dynamics of migraineurs to adapt breath holding task. For the analyses of cerebrovascular dynamics mainly two parameters are investigated: peak amplitude of the s(k) dur-

ing four breath holds and time to peak amplitude from beginning of the breath hold. The amplitude values grouped on the basis of breath holds and p values obtained by applying ANOVA test on filtered responses of six migraine and six subjects are demonstrated in Table 5.4. As seen from table, magnitudes of amplitudes belonging to migraineurs are supressed for all breath holds supporting the observation obtained in frequency domain. These results may be evident for the vasoconstrictive character of the cerebrovascular system of migraineurs.

Table 5.4
Amplitude values of averaged [Hb] data obtained from parametric identification for four breath holds (mean(std))

Breath holds	**Normal**	**Migraine**	**p value**
First	1.83 (1.03)	0.70 (1.05)	0.088
Second	2.00 (1.56)	-0.08 (1.03)	0.021
Third	2.11 (1.02)	0.28 (1.33)	0.023
Fourth	1.82 (1.05)	0.47 (0.79)	0.03

Time to peak parameter indicates time between the rise of [Hb] response and the start of breath hold. Table 5.5 demonstrates no significant difference between migraine and healthy subjects. This may show that both group members have approximately same oxygen consumption time although oxygen consumption rate is not same due to differences in peak amplitude. It is important to mention that determining the time to peak of migraineurs is difficult because of the fluctuating character of [Hb] signal during breath holds. Even in some cases, expected significant rise in [Hb] data could not visualized throughout analysis leading to a confusion in the time to peak parameter.

Table 5.5
Time to peak values of averaged [Hb] data obtained from parametric identification for four breath holds (mean(std))

Breath holds	**Normal**		**Migraine**		**p value**
First	28.50	(7.03)	35.13	(2.7)	0.056
Second	31.23	(7.66)	35.09	(2.05)	0.54
Third	32.46	(4.13)	34.06	(2.65)	0.44
Fourth	36.17	(16.06)	35.10	(2.44)	0.77

6. CONCLUSIONS

In this study, data acquired from healthy and migraine subjects with fNIRS during a breath holding task is analysed by using a parametric identification technique to investigate the cerebrovascular dynamics of migraine. Three modeling methodologies are followed to test the success of identification algorithm in modeling the brain hemodynamic response (BHR). First modeling scheme depicts the frequency intervals for four breath holds in which BHR of migraineurs differs from the healthy ones. Frequencies between 0.01 Hz and 0.03 Hz which correspond to rise in [Hb] data, are significantly different in two groups. Also, estimate power spectrum of migraneurs show diversity at 0.13 Hz and 0.25Hz. At these frequencies energy of the spectrum is found smaller in migraneurs relative to normals. Second modeling scheme depicts largeness in model orders of migraineurs relative to healthy subjects. Final modeling scheme is performed by using a reference signal obtained by averaging HBRs rather than a square wave. Results of this scheme show the supressed behavior of migraneurs' responses.

6.1 Recommendations for future work

Success of ARX modeling can be tested in synthetic trials composed by the superposition of background activity and mathematical functions that models [Hb] data during breath holding task. In the modeling procedure, responses which involve abrupt changes originating from motions of subjects, sometimes force higher model orders. This problem can be encountered by changing probe design to which would not affect from this motions.

Even though linear parametric modeling have been quite capable of capturing the BHRs of subjects, other modeling techniques involving non-linear and non parametric modeling or neural network analysis can improve both time and frequency domain analysis of BHR.

REFERENCES

1. McKinley, M., and V. O'Loughlin, *Human Anatomy*, McGraw-Hill, 1st ed., 2006.

2. Headache Classification Committee of the International Headache Society, "Classification and diagnostic criteria for headache disorders, cranial neuralgias and facial pain," *Cephalalgia*, Vol. 8, pp. 1–96, 1988.

3. Gerpen, J. A. V., S. Hickey, and D. J. Capobianco, "Migraine: Diagnosis, prevention and treatment." Jacksonville Medicine, April 2000.

4. Capobianco, D. J., W. P. Cheshire, and J. K. Campbell, "An overview of the diagnosis and pharmacologic treatment of migraine," *Mayo Clin Proc*, Vol. 71, no. 11, pp. 1055–1066, 1996.

5. Pryse-Phillips, W. E. M., D. W. Dodick, J. G. Edmeads, M. J. Gawel, R. F. Nelson, R. A. Purdy, G. Robinson, D. Stirling, and I. Worthington, "Guidelines for the diagnosis and management of migraine in clinical practice," *Can Med Assoc J*, Vol. 156, pp. 1273–1287, May 1997.

6. May, A., "The role of imaging in the pathophysiology and diagnosis of headache," *Curr Opin Neurol*, Vol. 18, no. 3, pp. 293–297, 2005.

7. Welch, K. M. A., "Current opinions in headache pathogenesis: introduction and synthesis," *Headache*, Vol. 11, no. 3, pp. 193–197, 1998.

8. Ferrari, M., "Migraine," *Lancet*, Vol. 351, pp. 1043–1051, 1998.

9. Wolff, H. G., and M. M. Tunis, "Analysis of cranial artery pressure pulse waves in patients with vascular headache of the migraine," *Trans Assoc Am Physician*, Vol. 65, no. 240–244, 1952.

10. Olesen, J., L. Friberg, T. S. Olsen, H. K. Iversen, N. A. Lassen, A. R. Andersen, and A. Karle, "Timing and topography of cerebral blood flow, aura and headache during migraine attacks," *Ann Neurol*, Vol. 28, pp. 791–798, 1990.

11. Merck Medicus, Medical Library, "Migraine pathophysiology." Avalaible: http://www.merckmedicus.com/pp/us/hcp/diseasemodules/searchmodules.jsp?pg=/pp/us/hcp/diseasemodules/migraine/pathophysiology.jsp.

12. Bussone, G., "Pathophysiology of migraine," *Neurol Sci*, Vol. 25, pp. 239–241, 2004.

13. University of Florida, College of Medicine, "Trigeminal nerve anatomy." Avalaible: http://medinfo.ufl.edu/year1/trigem/text.html.

14. Washington University, School of Medicine, "Somatosensory pathways from the face." Avalaible: http://thalamus.wustl.edu/course/face.html.

15. Loyola University of Chicago, School of Medicine, "Trigeminal nerve." Avalaible: http://www.meddean.luc.edu/lumen/meded/GrossAnatomy/h-n/cn/cn1/cn5.htm.

16. Bolay, H., and M. A. Moskowitz, "The neurobiology of migraine and transformation of headache therapy," in *Neuroscience, Molecular Medicine and the Therapeutic Transformation of Neurology* (Waxman, S., ed.), pp. 107–123, Elsevier, 2005.

17. Goadsby, P. J., L. Edvinsson, and R. Ekman, "Vasoactive peptide release in the extracerebral circulation of humans during migraine headache," *Ann Neurol*, Vol. 28, pp. 183–187, 1990.

18. Burstein, R., "Deconstructing migraine headache into peripheral and central sensitization," *Pain*, Vol. 89, pp. 107–110, 2001.

19. Moskowitz, M. A., "Pathophysiology of headache-past and present," *Headache*, Vol. 47, pp. 58–63, 2007.

20. Leao, A. A. P., "Spreading depression of activity in the cerebral cortex," *J Neurophysiol*, Vol. 7, pp. 359–390, 1944.

21. Hadjikhani, N., D. R. M. Sanchez, O. Wu, D. Schwartz, D. Bakker, B. Fischl, K. K. Kwong, F. M. Cutrer, B. R. Rosen, R. B. Tootell, A. G. Sorensen, and M. A. Moskowitz, "Mechanisms of migraine aura revealed by functional mri in human visual cortex," *Proc Natl Acad Sci USA*, Vol. 98, pp. 4687–4692, 2001.

22. Dalkara, T., N. T. Zervas, and M. A. Moskowitz, "From spreading depression to the trigeminovascular system," *Neurol Sci*, Vol. 27, pp. 86–90, 2006.

23. May, A., "A review of diagnostic and functional imaging in headache," *J Headache Pain*, Vol. 7, pp. 174–184, 2006.

24. Borsook, D., R. Burstein, E. Moulton, and L. Becerra, "Functional imaging of migraine and the trigeminal system," *Headache*, Vol. 46, pp. 32–38, 2006.

25. Wyatt, I. S., M. Cope, D. T. Delpy, C. E. Richardson, A. D. Edwards, S. C. Wray, and E. O. R. Reynolds, "Quantification of cerebral blood volume in newborn infants by near infrared spectroscopy," *J Physiol*, Vol. 68, pp. 1086–1091, 1990.

26. Elwell, C. E., M. Cope, A. D. Edwards, J. S. Wyatt, D. T. Delpy, and R. E. O. R, "Quantification of adult cerebral haemodynamics by near infrared spectroscopy," *J Appl Physiol*, Vol. 77, pp. 2753–2760, 1994.

27. Jobsis, F. F., "Noninvasive, infrared monitoring of cerebral and myocardial oxygen sufficiency and circulatory parameters," *Science*, Vol. 198, pp. 1264–1267, 1977.

28. Delpy, D. T., M. Cope, Z. P. van der Zee, S. Arridge, S. Wray, and J. Wyatt, "Estimation of optical pathlength through tissue from direct time of flight measurement," *Phys Med Biol*, Vol. 33, pp. 1433–1442, 1988.

29. Duncan, A., J. H. Meek, M. Clemence, C. E. Elwell, L. Tyszczuk, M. Cope, and D. T. Delpy, "Optical pathlength measurements on adult head, calf and forearm and the head of the newborn infant using phase resolved optical spectroscopy," *Phys Med Biol*, Vol. 40, pp. 295–304, 1995.

30. Akin, A., and D. Bilensoy, "Cerebrovascular reactivity to hypercapnia in migraine patients measured with near-infrared spectroscopy," *Brain Res*, Vol. 1107, pp. 206–214, 2006.

31. Akin, A., D. Bilensoy, U. E. Emir, M. Gulsoy, S. Candansayar, and H. Bolay, "Cerebrovascular dynamics of patients with migraine: Near-infrared spectroscopy study," *Neurosci Lett*, Vol. 400, pp. 86–91, 2006.

32. Liboni, W., F. Molinari, G. Allais, O. Mana, E. Negri, G. Grippi, C. Benedetto, G. D'Andrea, and G. Bussone, "Why do we need nirs in migraine?," *Neurol Sci*, Vol. 28, pp. 222–224, 2007.

33. Shinoura, N., and R. Yamada, "Decreased vasoreactivity to right cerabral hemisphere pressure in migraine without aura: a near infrared spectroscopy study," *Clin Neurophysiol*, Vol. 116, pp. 1280–1285, 2005.

34. Enqvist, M., *Linear Models of Nonlinear Systems.* PhD thesis, Linkopings Universitet, SE-581 83 Linkoping, Sweden, 2005.

35. Ljung, L., *System Identification Theory for the User*, Prentice Hall Ptr, 2nd ed., 1999.

36. Johansson, R., *System Modeling and Identification*, New Jersey: Prentice Hall, 1993.

37. Cerutti, S., G. Chiarenza, D. Liberati, P. Mascellani, and G. Pavesi, "A parametric method identification of single-trial event-related potentials in the brain," *IEEE Trans Biomed Eng*, Vol. 35, no. 9, pp. 701–711, 1988.

38. Liberati, D., S. D. Corrado, and S. Mandelli, "Topographic mapping of single-sweep evoked potentials in the brain," *IEEE Trans Biomed Eng*, Vol. 39, pp. 943–951, 1992.

39. Baraldi, P., A. Manginelli, M. Maieron, D. Liberati, and C. Porro, "An arx model-based approach to trial by trial identification of fmri-bold responses," *Neuroimage*, Vol. 37, pp. 189–201, 2007.

40. Bilensoy, D., "Cerebrovascular dynamics in migraine measured with fNIRS," Master's thesis, Bogazici University, Istanbul, Turkey, 2005.

41. Muller, M., and M. Marziniak, "The linear behavior of the system middle cerebral artery flow velocity and blood pressure in patients with migraine: Lack of autonomic control?," *Stroke*, Vol. 36, pp. 1886–1890, 2005.

42. Parker, M. J., "Breath-holding and its breakpoint," *Exp Physiol*, Vol. 91, pp. 1–15, 2006.

43. Molinari, F., W. Liboni, G. Grippi, and E. Negri, "Relationship between oxygen supply and cerebral blood flow assessed by transcranial doppler and near infrared spectroscopy in healthy subjects during breath holding," *J Neuroengineering Rehabil*, Vol. 3, no. 16, 2006. Available from: http://www.jneuroengrehab.com/content/3/1/16.

44. Obrig, H., M. Neufang, R. Wenzel, M. Kohl, J. Steinbrink, K. Einhaupl, and A. Villringer, "Spontaneous low frequency oscillations of cerebral hemodynamics and metabolism in human adults," *Neuroimage*, Vol. 12, pp. 623–639, 2000.

45. Hudetz, A. G., J. J. Smith, J. G. Lee, Z. J. Bosnjak, and J. P. Kampine, "Modification of cerebral laser-doppler flow oscillations by halothane, pco2, and nitric oxide synthase blockade," *Am J Physiol*, Vol. 269, pp. 114–120, 1995.

46. Biswall, B. B., K. J. Van, and J. S. Hyde, "Simultaneous assessment of flow and bold signals in resting-state functional connectivity maps," *NMR Biomed*, Vol. 10, pp. 165–170, 1997.

47. Elwell, C. E., H. Owen-Reece, J. S. Wyatt, M. Cope, E. O. Reynolds, and D. T. Delpy, "Influence of respiration and changes in expiratory pressure on cerebral haemoglobin concentration measured by near infrared spectroscopy," *J Cereb Blood Flow Metab*, Vol. 16, pp. 353–357, 1996.